Chapter 9

Preparation, Characterization, and Preliminary Biocompatibility Evaluation of Carbon Ion-Implanted Silicone Rubber

Xin Zhou, Yiming Zhang, Xiaohua Shi and Dongli Fan

Additional information is available at the end of the chapter

http://dx.doi.org/10.5772/intechopen.69251

Abstract

Silicone rubber (SR) is a common soft tissue filler material used in plastic surgery. However, it suffers from poor biocompatibility. Previous studies have found that the ion implantation technology can be used to improve the biocompatibility of metal materials. However, it is not clear whether it can improve the biocompatibility of polymer materials. In this study, carbon ion SR was prepared by carbon ion implantation. After that, the characteristics of ion implanted SR were investigated. Then, *Escherichia coli* was utilized to test the antibacterial ability of the carbon ion implanted SR. Besides, the dermal fibroblasts were used to evaluate the cytocompatibility. From the results, carbon ion implantation had no significant effect on the hardness, tensile strength and elongation at break of SR. At the same time, there was no significant change in the surface morphology of SR. But the results show that the surface nano-morphology, surface element composition, hydrophobic and ζ potential of the surface of SR changed significantly. The changes further mediated the lower adhesion of bacteria and enhanced biocompatibility. In conclusion, the carbon ion implantation technology can improve the surface properties of silicone rubber, and further improve its biocompatibility.

Keywords: silicone rubber, ion implantation, polymer, surface modification, biocompatibility

1. Introduction

In the clinical application of plastic surgery, silicone rubber (SR) due to its good physical and chemical stability, physical inertia, easy processing, and corrosion resistance is still the most commonly used clinical soft tissue filling material [1–4]. However, a strong hydrophobic SR surface, leading to its poor biocompatibility, the fibrous connective tissue, forms a capsule around the material [5]. The capsule thickening and contraction over time easily lead to deformation and displacement of implant materials. Besides, certain materials made from silicone rubber, such as catheters, are widely used in medicine but have several limitations, for example, bacteria can readily colonize the surfaces of silicone rubber, facilitating infection and even causing patient death in certain cases [6–9]. It is of significance to carry out suitable surface modification to enhance its biocompatibility and further to improve the clinical effect of soft tissue filling [10].

At present, the surface modification of silicone rubber can be treated by plasma treatment, grafting copolymerization, and biomimetic coating, but there are some defects, such as the steps were cumbersome and substrate temperature and the conditions are not easy to control [11–18]. In this study, the technology of ion implantation which is mainly used in metal and semiconductor materials is introduced into the surface modification of silicone rubber material. This technology has its unique advantages. The substrate temperature can be controlled, and there are a variety of ion sources that can be chosen and a micrographic structure that also can be formed on the surface of the material. At the same time, the ion implantation does not affect the bulk properties of material [19–21].

In this study, graphite was used as carbon source, and carbon ion was used to treat the surface of silicone rubber. Then, scanning electron microscope (SEM), Fourier transformation infrared spectroscopy (FTIR), X-ray diffraction (XRD), X-ray photoelectron spectroscopy (XPS), atomic force microscopy (AFM), water contact angle (WCA), ζ potential, Shore hardness A, elongation at break, and breaking strength were conducted to investigate the characteristics of modified silicone rubber. After that, *E. coli* was utilized to test the antibacterial ability of the carbon ion-implanted silicone rubber. Then, the dermal fibroblasts were used to evaluate the cytocompatibility through CCK-8, immunofluorescence, and WB. Furthermore, evaluation of tissue compatibility was carried out by the hematoxylin and eosin staining, Masson's staining, and immunohistochemistry test after the sample was subcutaneously implanted to SD rats for 7, 30, 90, and 180 days. The long-term goal of this study is to gain a better biomaterial for use by plastic surgeons or other clinical applications.

2. Materials and methods

2.1. Sample preparation

SR sheets with dimensions of 100 × 100 × 1 mm were prepared from a two-component silicone system. Both component A and component B were clinical-quality liquids provided

http://dx.doi.org/10.5772/intechopen.69251

by Chenguang Research Institute of Chemical Industry, China. Three doses of carbon ions were implanted using the ion implanter, respectively. The doses are 1×10^{15} ions/cm^2. After that, SR and C-SR sheets were manufactured into disc-like samples with a diameter of 6 mm using a hole puncher and into square samples with dimensions of 10 × 10 × 1 mm. The disc-like samples were used in in vitro antibacterial adhesion tests, and the square samples were used for in vivo tissue compatibility and in vitro cytocompatibility evaluation. All samples were sterilized with 75% alcohol overnight. In all experiments, SR is served as the control.

2.2. Characterization of carbon ion-implanted silicone rubber

2.2.1. Scanning electron microscopy

Clean the sample with ethanol, then place it in a 37° incubator, and let it dry. After that, put the sample into the vacuum pump and gold plating on the surface under the negative pressure state. After cooling, the surface morphology was observed by scanning electron microscope.

2.2.2. Fourier transformation infrared

Put clean and dry samples in Fourier transformation infrared spectrometer, and then set the wave number to 4 cm^{-1}; scan range is 400–4000cm^{-1}. The surface composition of the samples was measured.

2.2.3. X-ray photoelectron spectrometer

The samples were cleaned and put in the X-ray photoelectron spectrometer. The Al Kα as radiation source, press to collect photoelectron emission from the samples and the photoelectron spectrum. Then, the content of chemical elements on the surface of the material was analyzed.

2.2.4. X-ray diffraction

The materials to be tested were cleaned by ethanol and then put into the X-ray diffraction spectrometer and analysis crystal structure of the carbon ion-implanted silicone rubber.

2.2.5. Atomic force microscope

The sample are cleaned by ethanol before being scanned by the Environment-Controlled Scanning Probe Microscope (Nanonavi E-Sweep, NSK Ltd., Tokyo, Japan), and each sample was imaged with 5 × 5 μm scanned area. The surfaces were analyzed by measuring the average surface roughness (Ra) of five randomly chosen images per sample from selected areas of 1 × 1 μm under atomic force microscope (AFM) analysis software (NanoNavi II, SII Nano Technology Inc., Tokyo, Japan). Ra is defined as the average absolute deviation of the roughness irregularities from the mean line over one sampling length and gives a good general description of height variations. Three replicas were used.

2.2.6. Water contact angle

The contact angle of the prepared samples was measured by DSA100 contact angle measuring instrument; the selected liquid is distilled water. When measuring the contact angle of the sample, six different parts of the sample were selected and measured at least three times.

2.2.7. ζ Potential

After the samples are cleaned by ethanol, the surface zeta potentials of materials were measured with a Zeta Potential Analyzer (DelsaNano C, Beckman Coulter, Germany). The measurements were carried out in 1 mmol NaCl electrolyte solution and with standard particles for flat surface cell (Otsuka Electronics Co., Ltd., Japan). Each sample chooses five points, and each point is tested 20 times.

2.2.8. Shore hardness

The samples were washed with absolute ethanol and then measured by an A type of the Shore hardness tester; each sample was tested five times, and the average value was obtained.

2.2.9. Tear strength and elongation at break

After the samples are cleaned by ethanol, an electronic universal testing machine was used to gain parameters of the tear strength and elongation at break. Each sample was tested five times, and the average value was obtained.

2.3. Evaluation of antibacterial properties

2.3.1. Bacterial culture preparation

Gram-negative *E. coli* (ATCC 25922) was employed to bacterial experiments. The strains were streaked on blood agar plates from frozen stocks and grown for 24 h at 37°C in ambient air. The agar plates were then kept at 4°C until further use. For each experiment, one colony from an agar plate was inoculated into 10 ml of tryptone soy broth (TSB) and incubated for 24 h. The bacterial suspension was then added to 0.9% sterile sodium chloride to a final concentration of 1.5×10^6 colony-forming units per ml (CFU/ml), after which a McFarland standard was prepared (in practical terms, OD600 nm = 0.132). The samples were placed on 96-well culture plates and separately incubated in 200 μl of the bacterial suspension at 37°C for 1 or 24 h. After that, the plate colony counting, fluorescence staining, and scanning electron microscopy (SEM) observations were conducted.

2.3.2. Plate colony counting

After the sample incubation in bacterial culture for 1 and 24 h, the bacteria on each sample were gently rinsed with phosphate-buffered saline (PBS), respectively, and ultrasonically

http://dx.doi.org/10.5772/intechopen.69251

detached in 1 ml of PBS solution. The bacteria in the PBS were re-cultivated on agar plates for colony counting. The antibacterial rates were determined based on the following relationship: antibacterial rate (%) = (CFU of control−CFU of experimental groups)/CFU of control × 100%. This assay was performed in triplicate.

2.3.3. Fluorescence staining

After incubation for 1 and 24 h, the various samples were gently rinsed with PBS before staining the bacteria on the samples. The staining was performed by applying LIVE/DEAD® BacLight™ Bacterial Viability Kit (L7029, Molecular Probes®, OR, USA) for 15 min in darkness and was examined by laser scanning confocal microscopy (LEICA TCS SP5, Germany). The areas of green and red color in the pictures were then analyzed by using Image-Pro Plus version 6.0 (Media Cybernetics, Inc., USA) and then calculating the proportion of red coloration based on the following relationship: red proportion (%) = red area/(green area + red area) × 100%.

2.3.4. Scanning electron microscopy (SEM) observation

After bacterial incubation for 1 and 24 h, the samples were rinsed with PBS to remove free bacterial cells and then fixed in 2.5% glutaraldehyde for 3 h at room temperature. The samples were then progressively dehydrated in a series of ethanol solutions (15, 30, 50, 70, 80, 90, 95, and 100%) for 15 min each. After that, the specimens underwent critical-point drying and coating with a thin conductive layer of Au. Finally, the morphology and adhesion of the bacteria on the various samples were determined by SEM (VEGA 2 SEM, TESCAN Inc., Brno, Czech Republic).

2.4. In vitro cytocompatibility evaluation

2.4.1. Cell culture

The use of primary dermal fibroblasts derived from discarded human neonatal circumcision specimens and the institutional ethical committee of the Third Military Medical University, People's Republic of China, approved this study. Cells were routinely cultured in Dulbecco's Modified Eagle's Medium (DMEM, Gibco) supplemented with 10% FBS and incubated at 37°C in a humidified atmosphere supplied with 5% CO_2. Trypsin-EDTA (Gibco) was used to detach cells. The loading concentration of cells for all experiments was 5×10^4 cells/ml. Incubation conditions remained unchanged.

2.4.2. CCK-8

To study cell proliferation, primary dermal fibroblasts were seeded on the samples and cultured in DMEM supplemented with 10% FBS at 37°C in a humidified 5% CO_2 atmosphere. Primary dermal fibroblast viability was quantified by cell counting kit (CCK)-8 assay after 24 h

of incubation. The CCK-8 solution and the medium were mixed at a volume ratio of 1:10. A total of 1 ml of mixed solution was added into each well after removing the medium and reincubated for further 2 h. The optical density (OD) was measured at the wavelength of 450 nm by using microplate reader.

2.4.3. Immunocytochemical staining

Immunocytochemical staining was performed as described previously. Primary dermal fibroblasts were cultured on different samples for 24 h and then rinsed with PBS and fixed with 4% paraformaldehyde. Cells were incubated with 1% Triton X-100 for 20 min and blocked for 20 min with PBS containing 5% fetal calf serum and 0.1% bovine serum albumin (BSA; Sigma-Aldrich, St. Louis, MO, USA). Afterward, slides were incubated for 60 min with the Actin Tracker Green antibody (1:100; Beyotime Biotechnology, Shanghai, China). Finally, counterstaining of nuclei was performed with 4′, 6-diamidino-2-phenylindole (DAPI) (Biotium, Hayward, CA, USA) staining. Then, the cells were observed and photographed with a laser confocal scanning microscope (Leica TCS SP5, Germany).

2.4.4. Western blotting

The primary dermal fibroblasts were seeded on the samples for 24 h. Next, the cells were washed with ice-cold phosphate-buffered saline (PBS) and lysed with RIPA lysis buffer and protease inhibitor cocktail (Roche Diagnostics, Indianapolis, IN, USA). The lysates were sonicated for 4 s and were separated by centrifugation at 4°C and 14,000g for 2 min. Protein concentration was determined by a BCA protein assay kit. Aliquots of 40 μg of proteins from each treatment were separated by 10% sodium dodecyl sulfate-polyacrylamide gel electrophoresis and transferred onto polyvinylidene difluoride (PVDF) membranes (Millipore, Bedford, UK). After blocking with 10% instant nonfat dry milk for 2 h, the membranes were incubated with primary antibody (dissolved in phosphate-buffered saline Tween 20) overnight at 4°C followed by incubation with secondary antibody for 1 h at room temperature. The immunosignal was detected with the enhanced chemiluminescence detection system (Amersham Biosciences, Piscataway, MD, USA). The detail of primary antibody used in this study was listed in **Table 1**. As a loading control, glyceraldehyde-3-phosphate dehydrogenase (GAPDH) was probed and visualized.

Antibody name	Catalogue no.	Isotype	Dilution rate	Molecular weight (kDa)	Manufacturer
FAK	12636-1-AP	R	1:500	110	Proteintech
Vinculin	sc-7649	G	1:200	117	Santa
Talin	14168-1-AP	R	1:500	230	Proteintech
Zyxin	60254-1-Ig	M	1:500	78	Proteintech
Paxillin	10029-1-Ig	R	1:1000	68	Proteintech
GAPDH	MAB374	M	1:300	36	Millipore

Table 1. The detail of primary antibody used in this study.

2.5. In vivo tissue compatibility evaluation

2.5.1. Animals and surgery

This research was performed in accordance with the *Guide for the Care and Use of Laboratory Animals* published by the US National Institutes of Health (Washington, DC; National Academies Press, 2011), and all of the animal protocols were approved by the Institutional Animal Care and Use Committee of the Third Military Medical University, China. A total of 16 female Sprague-Dawley rats (weighing 160–200 g) were used (2 groups of 8 animals each), and all rats were housed under a 12-h light/dark cycle with free access to water and food. Prior to surgery, all of the rats were anesthetized with 3% pentobarbital sodium (1 ml/1000 g). The skin was swabbed with iodine, and four parallel incisions (10 mm) were performed. The material samples were implanted subcutaneously along the back region. The implants and their surrounding tissue were retrieved from each group by wide excision at 7, 30, 90, and 180 days after implantation and were then fixed in 4% paraformaldehyde solution. After that, HE and Masson's staining and immunohistochemistry were conducted.

2.5.2. HE and Masson's staining

The fixed tissues were sectioned (6 μm thick) and stained using a HE Staining Kit (C0105, Beyotime Inc., Shanghai, China). The thickness of the fibrotic capsule around each implant was determined at five equidistant points for statistical accuracy. Collagen deposition in the tissue around the implants was studied by Masson's trichrome staining, which was performed using a staining kit (MST-8003, Maixin Biological Technology Co., Ltd., Fujian, China). All procedures were performed based on the manufacturer's instructions.

2.5.3. Immunohistochemistry

Immunohistochemistry was performed on 4% paraformaldehyde-fixed cryostat sections of frozen tissue specimens. Endogenous peroxidase and nonspecific antibody binding were blocked with 3% H_2O_2 and 100% methanol, with a ratio of 1:5 and a blocking time of 30 min. Next, 0.02 M PBS was used for antigen retrieval while heating in a water bath, followed by treatment with 5% blocking reagent at 37°C for 30 min. The slides were then incubated at 4°C for 12 h with a primary antibody against CD68, CD4, TNF-α, α-SMA, or elastin (1:25) (Boster Biological Engineering Co., Ltd., Hubei, China). After washing in PBS, a secondary antibody was applied for 30 min. Visualization was achieved by adding 3, 3′-diaminobenzidine chromogen.

2.6. Statistics

All data are expressed as the mean ± standard deviation (SD); statistics were analyzed using SPSS statistical software. One-way ANOVA combined with multiple comparisons performed along with Tukey's multiple comparison tests was utilized to determine the level of significance. In all of the statistical evaluations, $P < 0.05$ was considered significant.

3. Results

3.1. Ion implantation changes the surface roughness and zeta potential of SR

After ion implantation, SEM, AFM, FTIR, XPS, XRD, water contact angle measure instrument, zeta potential detection instrument, Shore A durometer, and an electronic universal testing machine were used to investigate the change in properties of carbon ion silicone rubber.

The SEM results failed to find any significant differences between virgin SR and three C-SRs (**Figure 1**), indicating that carbon ion implantation did not change the macroscale surface of SR.

At the same time, there are no any significant differences, or the difference was very small on the results of FTIR (**Figure 2**), XRD (**Figure 3**), Shore hardness (**Figure 4A**), tear strength (**Figure 4B**),

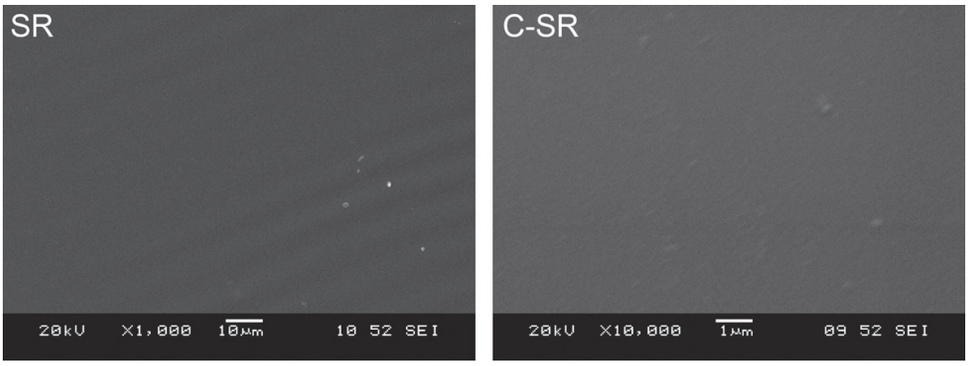

Figure 1. Representative scanning electron microscopic images of virgin silicone rubber and carbon ion-implanted silicone rubber.

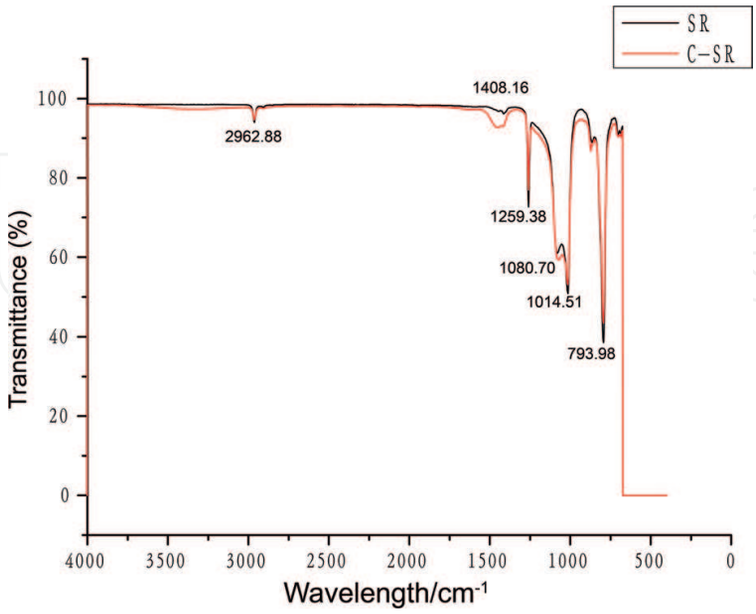

Figure 2. The Fourier transformation infrared spectroscopy results of virgin silicone rubber and carbon ion-implanted silicone rubber.

http://dx.doi.org/10.5772/intechopen.69251

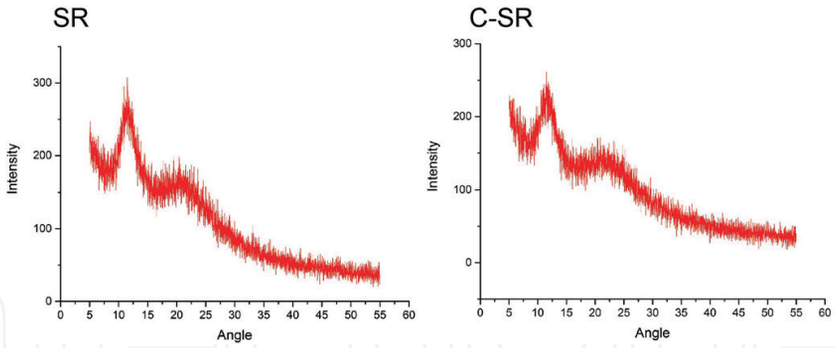

Figure 3. The XRD results of virgin silicone rubber and carbon ion-implanted silicone rubber.

and elongation at break (**Figure 4C**). The FTIR showed that there has been no new peak, noting that there has been no functional group produced. The Shore hardness, tear strength, and elongation at break showed that the ion implantation cannot change the bulk properties.

From the results of water contact angle, we found that carbon ion implantation significantly decreased the water contact angle of SR (**Figure 5**).

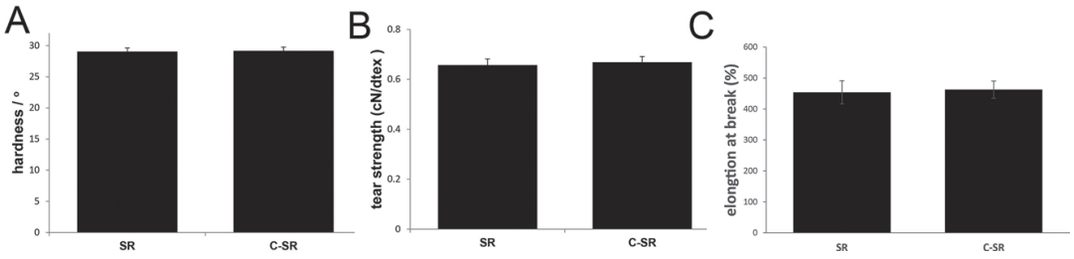

Figure 4. The mechanical properties of virgin silicone rubber and carbon ion-implanted silicone rubber. (A) Shore hardness. (B) Tear strength. (C) Elongation at break.

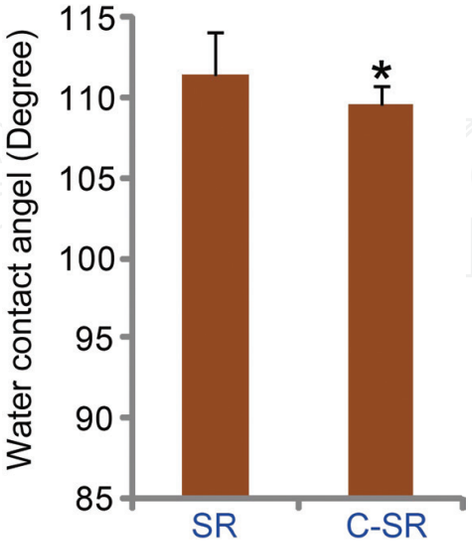

Figure 5. Water contact angle of virgin silicone rubber and carbon ion-implanted silicone rubber. (*$P < 0.05$ compared with silicone rubber).

Besides, the XPS results showed that carbon ion implantation significantly changed the surface silicone oxygen rate and chemical element distribution of SR (**Figure 6**) (**Table 2**); note that with the ion implantation, the carbon content in the material increased, while the Si content decreased, suggesting that implanted carbon atom may replace the Si of virgin SR, interrupting the original Si-O assemble, so the surface-free energy increases, thereby theoretically decreasing material's water contact angle. Furthermore, AFM images revealed that the surfaces of C-SRs were composed of larger irregular peaks and deeper valleys, while virgin SR exhibited a relatively smooth and more homogeneous surface (**Figure 7A**). The surface roughness of the CSR, which underwent carbon ion implantation, was the highest (**Figure 7B**).

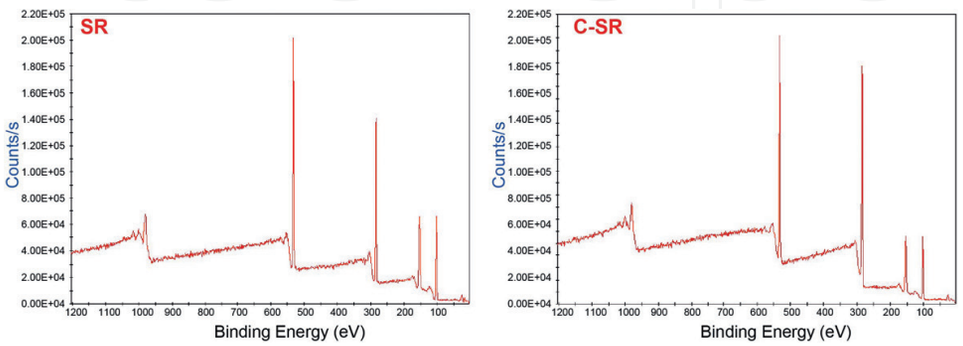

Figure 6. XPS results of virgin silicone rubber and carbon ion-implanted silicone rubber.

Group	Si 2p	C 1s	O 1s
SR	28.82	47.57	23.65
C-SR	18.94	58.40	22.67

Table 2. Chemical composition (in at.%) from the XPS analysis.

In addition, all samples exhibited negative zeta potentials and reflect that the surfaces of all samples were negatively charged. The absolute value of the zeta potential increased with the ion dose (**Figure 8**). Considering the influence of surface roughness on contact angle, we propose that ion implantation can change the surface roughness of the material and increase the surface potential of the material.

3.2. Ion implantation inhibits bacterial adhesion on SR

Preventing bacterial adhesion and biofilm formation by improving the surface antibacterial adhesion property of the silicone rubber is critical for eliminating various types of infections. After ion implantation, we use Gram-negative *E. coli* (American Type Culture Collection 25922) to evaluate the ability to resist bacteria adhesion. From the result, after 1 h of incubation, the rate of *E. coli* adherence on the carbon ion silicone rubber increased to approximately 11% (**Figure 9**) ($P < 0.05$). After 24 h of incubation, the rates of bacterial adherence were slightly lower, but did not significantly decrease compared with that after 1 h of incubation ($P > 0.05$).

http://dx.doi.org/10.5772/intechopen.69251

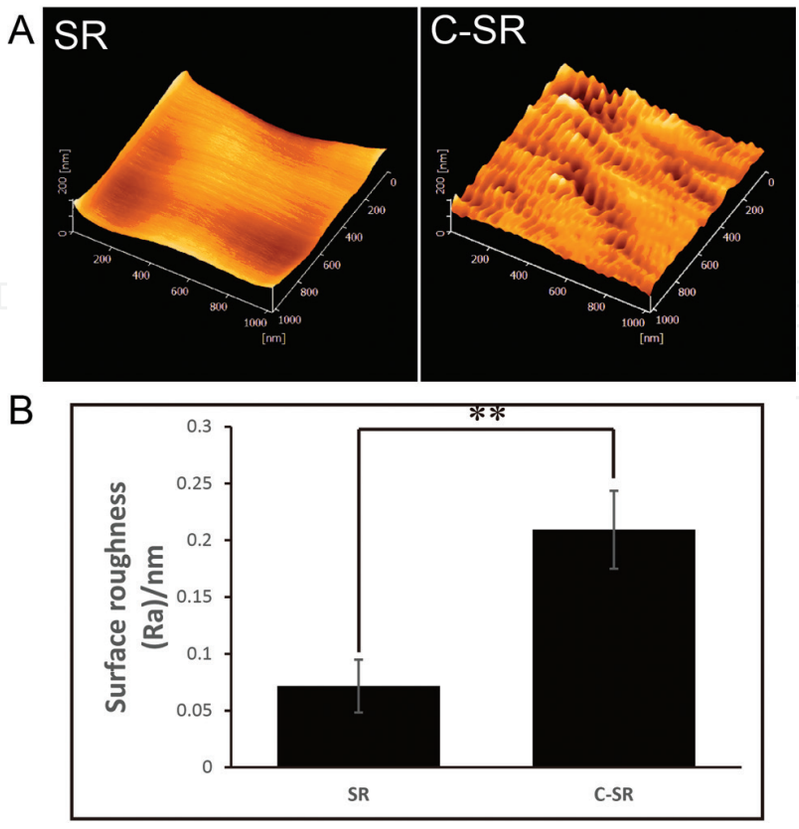

Figure 7. AFM results of virgin silicone rubber and carbon ion-implanted silicone rubber. (A) Representative atomic force microscope images. (B) Surface roughness. (**P < 0.01 compared with silicone rubber).

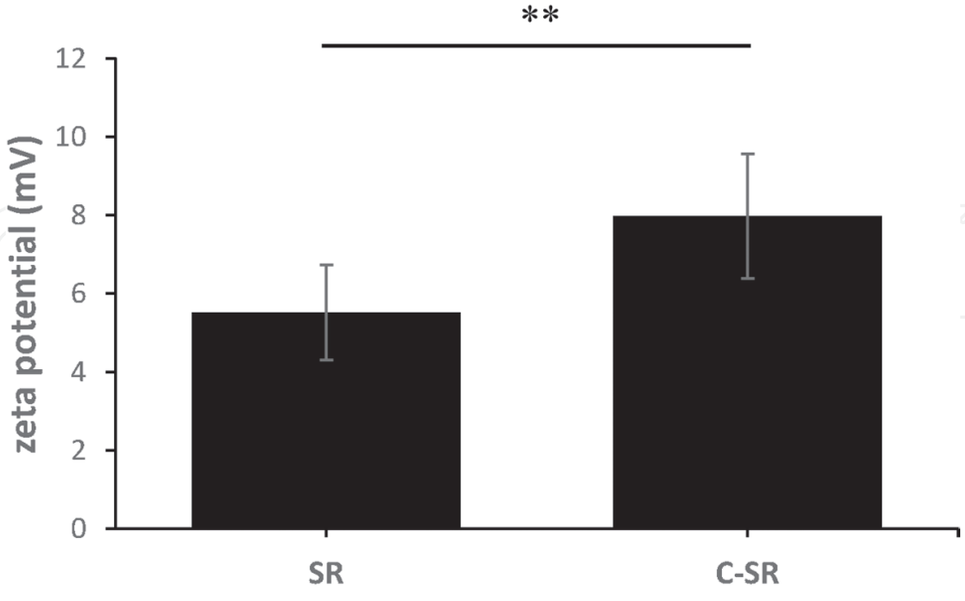

Figure 8. Zeta potential of virgin silicone rubber and carbon ion-implanted silicone rubber. (**P < 0.01 compared with silicone rubber).

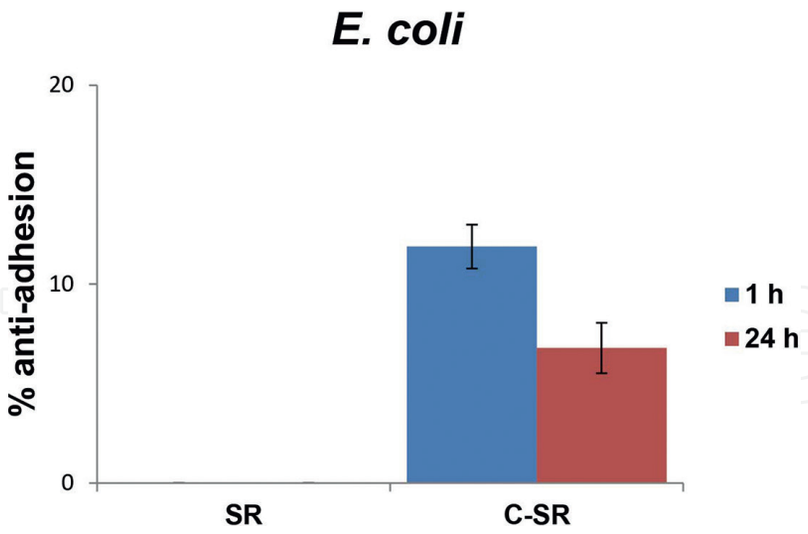

Figure 9. The antiadhesion rates (percentage) of virgin silicone rubber and carbon ion-implanted silicone rubber. After all samples were cultured in bacterial suspension for 1 and 24 h, bacteria on the surface of all samples were recultured on the plate, and bacterial colonies were subsequently counted. According to the number of colonies, the antiadhesion rates (percentage) for *E. coli* were counted. The data are presented as the mean ± SD (n = 3); $^{*}P < 0.05$ compared with silicone rubber.

The ability of carbon ion silicone rubber to prevent viable bacteria colonization was also verified by fluorescence staining. The results showed that the amount of bacterial adhesion to the surface of carbon ion silicone rubber was reduced compared with the virgin silicone rubber (**Figure 10**).

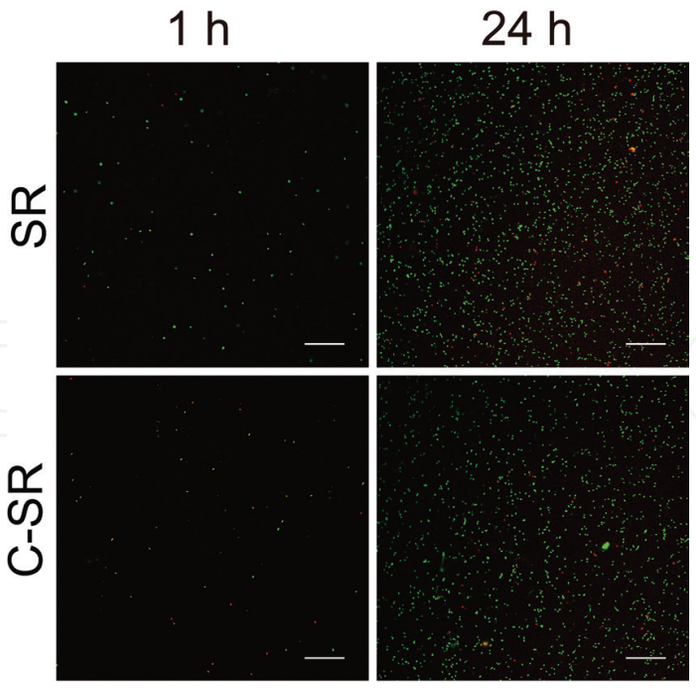

Figure 10. Representative images of fluorescence staining observation of virgin silicone rubber and carbon ion-implanted silicone rubber. Representative images showing bacteria viability on SR and C-SR after 24 h of incubation, as indicated by staining with a LIVE/DEAD BacLight Bacterial Viability Kit (Thermo Fisher Scientific, Waltham, Mass.). The live bacteria appear green, whereas the dead bacteria are red (original magnification, ×200).

Scanning electron microscopy was performed to examine the attached bacteria. The results showed that bacteria were observed on surfaces of all samples, but there were differences in quantity (**Figure 11**).

3.3. Ion implantation enhances the cell proliferation and adhesion on SR

Cell adhesion and proliferation were evaluated by the immunofluorescence, WB, and CCK-8 experiments. After cell culture on samples for 24 h, the cell adhesion was reflected by the immunofluorescence and focal adhesion kinase (FAK), and adhesion-associated proteins vinculin, talin, zyxin, and paxillin were also detected by WB. As shown in **Figure 12**, primary dermal fibroblasts cultured on C-SRs have a higher adherence rate and higher cell areas.

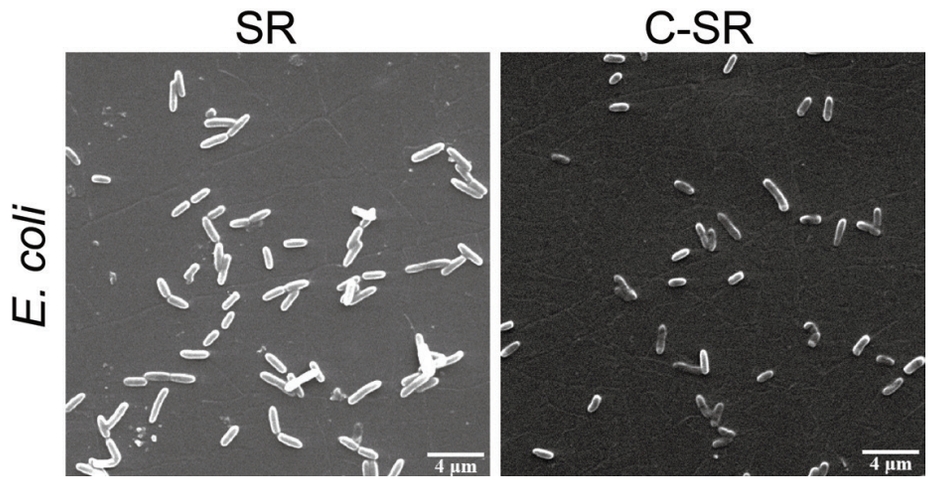

Figure 11. Representative scanning electron microscopic images of the bacteria on SR and C-SR after incubation for 24 h.

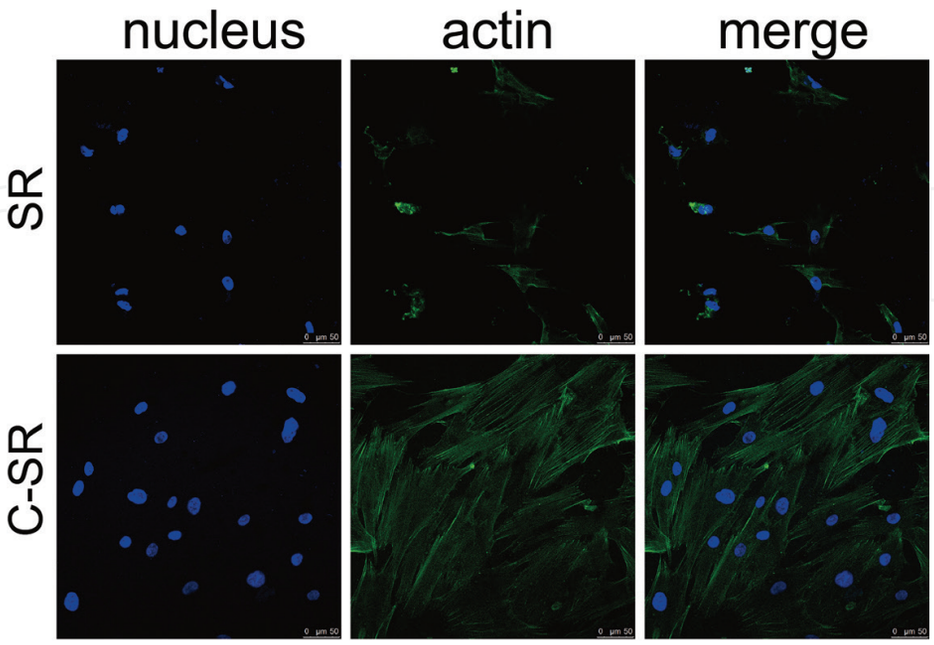

Figure 12. Representative cytoskeleton images of the fibroblasts on SR and C-SR after incubation for 24 h.

The WB results also showed that the primary dermal fibroblasts cultured on C-SR expressed higher levels of FAK and adhesion-associated proteins vinculin, talin, zyxin, and paxillin (**Figure 13**).

Besides, the cell proliferation was higher on C-SR (**Figure 14**). These results together indicate that carbon ion implantation could provide a better environment for cell adhesion and proliferation.

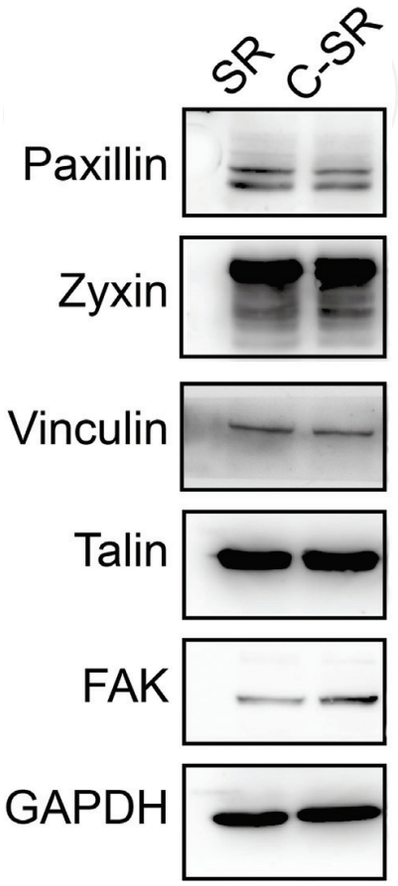

Figure 13. The WB results of FAK and adhesion-associated proteins vinculin, talin, zyxin, and paxillin.

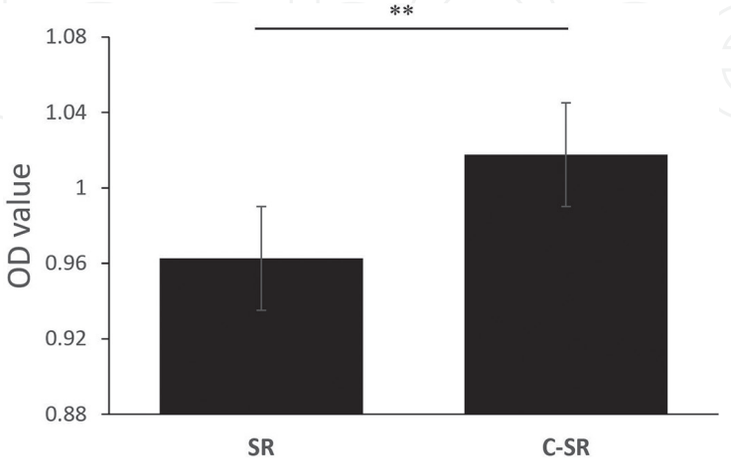

Figure 14. Cell proliferation on SR and C-SR after incubation for 24 h.

http://dx.doi.org/10.5772/intechopen.69251

3.4. Ion implantation enhances the tissue compatibility of SR

After ion implantation, the host responses were evaluated by surveying inflammation and fibber capsule formation that developed after subcutaneous implantation in Sprague-Dawley rats for 7, 30, 90, and 180 days. The thickness values of tissue capsules around the implants were identified from hematoxylin and eosin-stained sections of the peri-implant soft tissues and were analyzed as one of the physiologic responses to implantation. At 7 days after implantation, silicone rubber had the thinnest tissue capsules, and carbon ion silicone rubber had thicker (**Figure 15**) ($P > 0.05$) and weaker tissue capsules. Interestingly, the thickness decreased with longer implantation (**Figure 15**). At 180 days after implantation, silicone rubber and C-SR had the thickest and the thinnest tissue capsules, respectively (**Figure 15**).

In addition, collagen deposition was revealed using Masson's trichrome staining. Our results show that collagen gradually became sparser over time and with increasing carbon ion doses. Carbon ion silicone rubber had obviously lower collagen deposition than silicone rubber (**Figure 16**) ($P < 0.05$).

To gain insight into inflammatory foreign body responses and capsule contracture to the samples, the major biomarkers CD68, CD4, tumor necrosis factor-α, elastin, and α-smooth muscle actin were detected using immunohistochemistry. The results showed that all samples present lower expression of CD68, with no significant differences. The distribution of CD4 in the inflammatory infiltrate, which was induced by the samples, was investigated to further understand the local immunomodulation against these types of materials. The results show that there were many positive staining areas of CD4 in silicone rubber after 90 days, but positive staining in the carbon ion silicone rubber decreased with time. After 90 days, CD4 significantly decreased compared with silicone rubber.

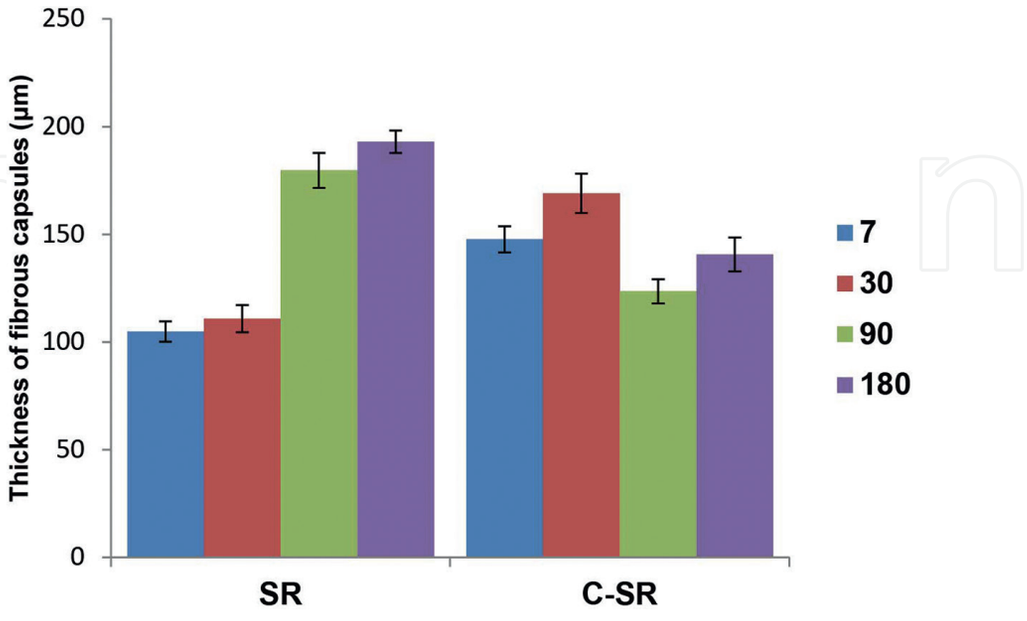

Figure 15. The capsule thicknesses around the implants.

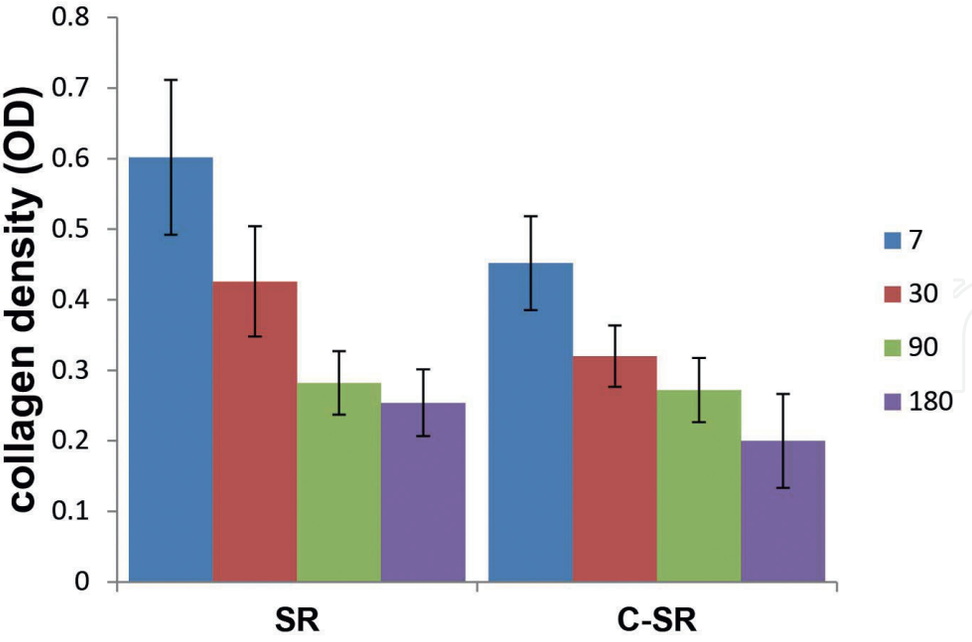

Figure 16. The collagen density around the implants.

In addition, the expression results of pro-inflammatory cytokine tumor necrosis factor-α by macrophage cells show that silicone rubber had an obviously positive staining area (**Table 3**).

Furthermore, the positive staining areas of α-smooth muscle actin and elastin have no difference; the positive staining area of α-smooth muscle actin appeared predominantly in silicone rubber than in carbon ion silicone rubber (**Table 4**). Elastin was intensely expressed in silicone rubber, particularly after 30 days (**Table 5**).

	7 days	30 days	90 days	180 days
SR	++	++	+++	+++
C1-SR	++	++	+	+

Table 3. Semiquantitative evaluation of TNF-α in peri-implant tissue.

	7 days	30 days	90 days	180 days
SR	+	++	++	++
C1-SR	+	+	+	+

Table 4. Semiquantitative evaluation of α-SMA in peri-implant tissue.

	7 days	30 days	90 days	180 days
SR	++	+++	+++	++
C1-SR	+	++	++	+

Table 5. Semiquantitative evaluation of elastin in peri-implant tissue.

4. Discussion

SR is the main method for the treatment of deformities and defects of body surface tissues and organs due to congenital or trauma. However, the SR material has poor cytocompatibility; cells are not easy to adhere to the surface of the material. It easy to form the fiber capsule on the surface, at the same time, deformation, displacement, and even cause skin infection and ulceration. By modifying the surface of SR and obtaining the modified SR material with good biocompatibility which it is expected to further improve the clinical therapeutic effect [22–25]. In this study, C ion implantation was used to modify SR. The surface properties of the materials were analyzed by a series of characterization techniques. The bacterial adherence and cell compatibility of C-SR were also observed. At the same time, a preliminary study on the histocompatibility was also carried out.

After C ion implantation, the surface properties of the material changed. The surface properties of materials can affect the biocompatibility of materials. In the further study, we observed the biocompatibility of the modified materials. CCK-8 test showed that the proliferation of human dermal fibroblasts on C-SR surface was better than that of SR. The adhesion of cells on the surface of materials mainly depends on the formation of adhesion complex. In this study, we found that the adhesion complex on C-SR had higher expression. These results indicated that C-SR was more favorable for cell adhesion and growth than SR; C-SR has excellent biocompatibility.

In this study, the surface properties and cell compatibility of modified C-SR were observed and analyzed. It was found that the surface properties of the modified materials changed somewhat compared with that of SR after carbon ion implantation. It is mainly because of the formation of new morphologies on the surface of SR after ion implantation; the change of surface properties may affect the hydrophobicity of material surface and improve the adsorption ability of the material to extracellular matrix proteins, so as to promote cell adhesion and proliferation on the surface of the material. Further studies also showed that C-SR was more favorable for cell adhesion and proliferation than SR. This suggests that if the modified material is implanted in the body, it will have a good affinity with the surrounding tissue, can reduce the degree of formation of the surrounding material, and can also reduce the deformation and displacement of the implant material and other complications. It can be concluded from the results that C ion implantation technology can improve the biocompatibility of polymer materials, and C-SR has great application prospect.

5. Conclusion

Our study evaluates the in vitro antibacterial properties and the in vivo host response to carbon ion-implanted silicone rubber. The results of our study indicate that the carbon ion silicone rubbers have good biocompatibility and lower bacterial adhesion and lower foreign body reaction with relatively thin fibrous capsules. All results show that ion implantation should be considered for further investigation and application, and carbon ion-implanted silicone rubber might be a better biomaterial for decreasing silicone rubber-initiated complications.

Acknowledgements

This work was funded by grants from the National Natural Science Foundation of China (81571918, 81401610) and a grant for Scientific Personnel Innovation from Chongqing (cstc2013kjrc-qnrc10003).

Author details

Xin Zhou, Yiming Zhang, Xiaohua Shi and Dongli Fan*

*Address all correspondence to: fdltmmu@sina.com

Department of Plastic and Cosmetic Surgery, Xinqiao Hospital, Third Military Medical University, Chongqing, China

References

[1] Liu P, Chen Q, Yuan B, Chen M, Wu S, Lin S, SHEN J. Facile surface modification of silicone rubber with zwitterionic polymers for improving blood compatibility. Materials Science & Engineering C-Materials for Biological Applications. 2013;**33**(7):3865-3874. DOI: 10.1016/j.msec.2013.05.025

[2] Lugowski SJ, Smith DC, Bonek H, Lugowski J, Peters W, Semple J. Analysis of silicon in human tissues with special reference to silicone breast implants. Journal of Trace Elements in Medicine and Biology. 2000;**14**(1):31-42. DOI: 10.1016/S0946-672X(00)80021-8

[3] Erlich MA, Parhiscar A. Nasal dorsal augmentation with silicone implants. Facial Plastic Surgery. 2003;**19**(4):325-330. DOI: 10.1055/s-2004-815652

[4] Cazacu M, Racles C, Vlad A, Antohe M, Forna N. Silicone-based composite for relining of removable dental prosthesis. Journal of Composite Materials. 2009;**43**(10):2045-2055. DOI: 10.1177/0021998309340447

[5] Anderson JM, Rodriguez A, Chang DT. Foreign body reaction to biomaterials. Seminars in Immunology. 2008;**20**(2):86-100. DOI: 10.1016/j.smim.2007.11.004

[6] Vasilev K, Cook J, Griesser HJ. Antibacterial surfaces for biomedical devices. Expert Review of Medical Devices. 2009;**6**(5):553-567. DOI: 10.1586/erd.09.36

[7] Bazaka K, Jacob MV, Crawford RJ, Ivanova EP. Plasma-assisted surface modification of organic biopolymers to prevent bacterial attachment. Acta Biomaterialia. 2011;**7**(5):2015-2028. DOI: 10.1016/j.actbio.2010.12.024

[8] Bergmann PA, Tamouridis G, Lohmeyer JA, Mauss KL, Becker B, Knobloch J, Mail Nder P, Siemers F. The effect of a bacterial contamination on the formation of capsular contracture with polyurethane breast implants in comparison with textured silicone implants: An animal study. Journal of Plastic Reconstructive and Aesthetic Surgery. 2014;**67**(10):1364-1370. DOI: 10.1016/j.bjps.2014.05.040

[9] Tang CY, Chen D-z, Chan KYY, Chu KM, Ng PC, Yue TM. Fabrication of antibacterial silicone composite by an antibacterial agent deposition, solution casting and crosslinking technique. Polymer International. 2011;**60**(10):1461-1466. DOI: 10.1002/pi.3102

[10] Rohrich RJ. Advances in breast augmentation. Plastic and Reconstructive Surgery. 2006;**118**(7):1S-2S. DOI: 10.1097/01.prs.0000247292.96867.06

[11] Xue L, Zhang Y, Zuo Y, Diao S, Zhang J, Feng S. Preparation and characterization of novel UV-curing silicone rubber via thiol-ene reaction. Materials Letters. 2013;**106**(1):425-427. DOI: 10.1016/j.matlet.2013.05.084

[12] van der Houwen EB, Kuiper LH, Burgerhof JG, van der Laan BF, Verkerke GJ. Functional buckling behavior of silicone rubber shells for biomedical use. Journal of the Mechanical Behavior of Biomedical Materials. 2013;**28**(1):47-54. DOI: 10.1016/j.jmbbm.2013.07.002

[13] Abbasi F, Mirzadeh H, Katbab AA. Modification of polysiloxane polymers for biomedical applications: A review. Polymer International. 2001;**50**(12):1279-1287. DOI: 10.1002/pi.783

[14] Magennis EP, Hook AL, Williams P, Alexander MR. Making silicone rubber highly resistant to bacterial attachment using thiol-ene grafting. ACS Applied Materials & Interfaces. 2016;**8**(45):30780-30787. DOI: 10.1021/acsami.6b10986

[15] Ziraki S, Zebarjad SM, Hadianfard MJ. A study on the role of polypropylene fibers and silica nanoparticles on the compression properties of silicone rubber composites as a material of finger joint implant. International Journal of Polymeric Materials and Polymeric Biomaterials. 2017;**66**(1):48-52. DOI: 10.1080/00914037.2016.1180623

[16] Rahman CV, Ben-David D, Dhillon A, Kuhn G, Gould TWA, Muller R, Rose F, Shakesheff KM, Livne E. Controlled release of BMP-2 from a sintered polymer scaffold enhances bone repair in a mouse calvarial defect model. Journal of Tissue Engineering and Regenerative Medicine. 2014;**8**(1):59-66. DOI: 10.1002/term.1497

[17] Ling T, Lin J, Tu JJ, Liu SQ, Weng WJ, Cheng K, Wang HM, Du PY, Han GR. Mineralized collagen coatings formed by electrochemical deposition. Journal of Materials Science-Materials in Medicine. 2013;**24**(12):2709-2718. DOI: 10.1007/s10856-013-5028-9

[18] Meretoja VV, Rossi S, Peltola T, Pelliniemi LJ, Narhi TO. Adhesion and proliferation of human fibroblasts on sol-gel coated titania. Journal of Biomedical Materials Research Part A. 2010;**95A**(1):269-275. DOI: 10.1002/jbm.a.32829

[19] Tsuji H, Izukawa M, Ikeguchi R, Kakinoki R, Sato H, Gotoh Y, Ishikawa J. Surface treatment of silicone rubber by carbon negative-ion implantation for nerve regeneration. Applied Surface Science. 2004;**235**(1):182-187. DOI: 10.1016/j.apsusc.2004.05.121

[20] Tsuji H, Sommani P, Hattori M, Yamada T, Sato H, Gotoh Y, Ishikawa J. Negative ion implantation for pattering mesenchymal-stem cell adhesion on silicone rubber and differentiation into nerve cells with keeping their adhesion pattern. Surface and Coatings Technology. 2009;**2003**(17-18):2562-2565. DOI: 10.1016/j.surfcoat.2009.02.076

[21] Tsuji H, Sommani P, Kitamura T, Hattori M, Sato H, Gotoh Y, Ishikawa J. Nerve-cell attachment properties of polystyrene and silicone rubber modified by carbon negative-ion implantation. Surface and Coatings Technology. 2007;**201**(19-20):8123-8126. DOI: 10.1016/j.surfcoat.2006.01.074

[22] Baba K, Hatada R, Flege S, Ensinger W. Preparation and properties of Ag-containing diamond-like carbon films by magnetron plasma source ion implantation. Advances in Materials Science and Engineering. 2012;**2012**(1):536853. DOI: 10.1155/2012/536853

[23] Dudognon J, Vayer M, Pineau A, Erre R. Mo and Ag ion implantation in austenitic, ferritic and duplex stainless steels: A comparative study. Surface and Coatings Technology. 2008;**203**(1-2):180-185. DOI: 10.1016/j.surfcoat.2008.08.069

[24] Fang J, Zhao JH, Sun Y, Ma HY, Yu XL, Ma Y, Ni YX, Zheng L, Zhou YM. Biocompatibility and antibacterial properties of zinc-ion implantation on titanium. Journal of Hard Tissue Biology. 2014;**23**(1):35-43

[25] Hou XG, Wang XM, Luan WJ, Li DJ, Dong L, Ma J. Study of antibacterial, hydrophilic and nanomechanical properties of TiOx films modified by Ag + beam implantation. Surface and Coatings Technology. 2013;**229**:71-75. DOI: 10.1016/j.surfcoat.2012.04.092